Supplemental materials

Strain-modulated Slater-Mott crossover of pseudospin-half square-lattice in $(SrIrO_3)_1/ (SrTiO_3)_1$ superlattices

Junyi Yang[1], Lin Hao[1], Derek Meyers[2], Tamene Dasa[3], Liubin Xu[3], Lukas Horak[4], Padraic Shafer[5], Elke Arenholz[5,6], Gilberto Fabbris[7], Yongseong Choi[7], Daniel Haskel[7], Jenia Karapetrova[7], Jong-Woo Kim[7], Philip J. Ryan[7], Haixuan Xu[3], Cristian D. Batista[1], Mark P. M. Dean[2], Jian Liu[1]

1.Department of Physics and Astronomy, University of Tennessee, Knoxville, Tennessee 37996, USA;

2. Department of Condensed Matter Physics and Materials Science, Brookhaven National Laboratory, Upton, New York 11973 USA.

3. Department of Material Science and Engineering, University of Tennessee, Knoxville, Tennessee 37996, USA;

4. Department of Condensed Matter Physics, Charles University, Ke Karlovu 5, 121 16 Prague, Czech Republic;

5. Advanced Light Source, Lawrence Berkeley National Laboratory, Berkeley, CA 94720, USA

6. Department of Materials Science & Engineering, University of California, Berkeley, CA 94720, USA;

7. Advanced Photon Source, Argonne National Laboratory, Argonne, IL, 60439 USA

1. Magnetization measurements.

We measured the magnetization of SL-LSAT using a commercial Quantum Design vibrating sample magnetometer. Figure S1 shows the temperature dependence of the remnant magnetization of SL-LSAT. An in-plane net magnetization is observed when temperature is below 75 K. The remnant magnetization (ReM) at 10 K is about 50% of that in SL-STO [1], consistent with the estimated AFM order parameter reduction from the magnetic resonant scattering experiments in the main text. On the other hand, we were not able to characterize the remnant magnetization of SL-NGO, because of the difficulty in eliminating the paramagnetic contribution from the NGO substrate that dominates the total signal in magnetization measurements.

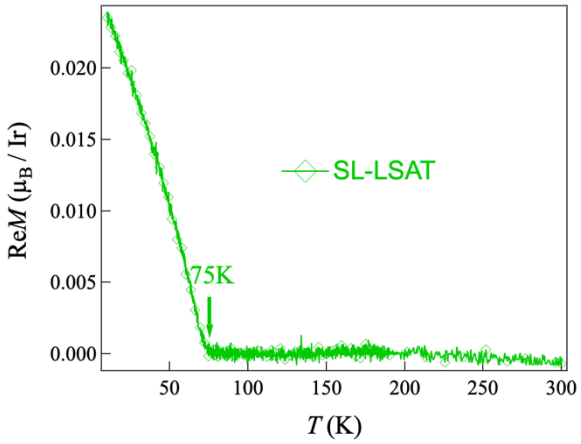

FIG. S1. Temperature dependence of the in-plane remnant magnetization of SL-LSAT. The remnant magnetization was measured under zero field after cooling down in a 0.5 T in-plane magnetic field.

2. X-ray resonant magnetic scattering measurements.

Figure S2(a) shows one representative energy profile at the (0.5 0.5 2) magnetic reflection of the SL-STO across the Ir L_3-edge. A clear resonant effect can be seen at energies slightly lower than the Ir L_3-edge white line, a common feature in magnetic iridate compounds

[1-6], demonstrating the dominant role of iridium ions in developing the magnetic long-range order. In the subsequent measurements, the x-ray energy was fixed at the value that maximizes the resonant effect. Figures S2(b-d) show *L*-scan around the (0.5 0.5 2) magnetic reflections for the SL-STO, SL-LSAT and SL-NGO, respectively.

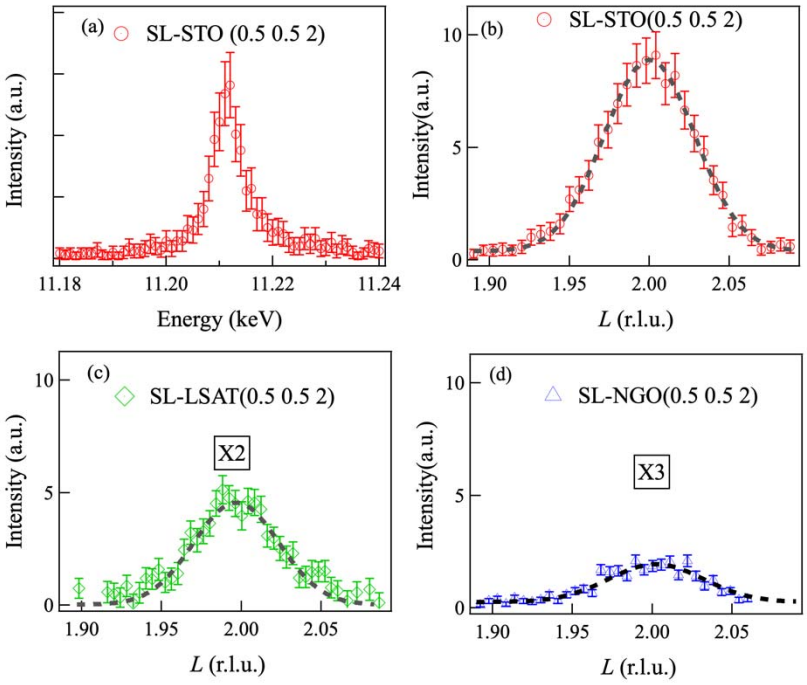

FIG. S2. (a) The energy profile at the (0.5 0.5 2) Bragg reflection across the Ir L_3-edge for the SL-STO at 7 K. *L*-scan (Ir L_3-edge) across the (0.5 0.5 2) magnetic reflection of SL-STO (b), SL-LSAT (c), and SL-NGO (d) at 7 K. The peak intensities of SL-LSAT and SL-NGO were plotted in the same scale as SL-STO for comparison and scaled by two and three times, respectively, for better visibility. The error bar denotes statistical error. The dash line serves a guide to the eyes.

3. Characterization of IrO_6/TiO_6 octahedral tilting and rotation through synchrotron XRD measurements.

The in-plane compressive strain may change IrO_6/TiO_6 octahedral tilting and rotation. Figures S3(a)-(c) show *L*-scan around the (0.5 1.5 5) Bragg reflection of SL-STO, SL-LSAT and

SL-NGO, respectively. Figure S3(d) shows *L*-scan around (0.5 0.5 5) of all the SLs. For SL-STO, a peak can be observed at (0.5 0.5 5), indicates a finite octahedra tilting [7]. On the other hand, no observable (0.5 0.5 5) peak was found for the SL-LSAT and SL-NGO (the non-zero background is the tail of the strong substrate peak), indicates that increasing compressive strain suppresses the octahedra tilting which becomes too weak to be seen.

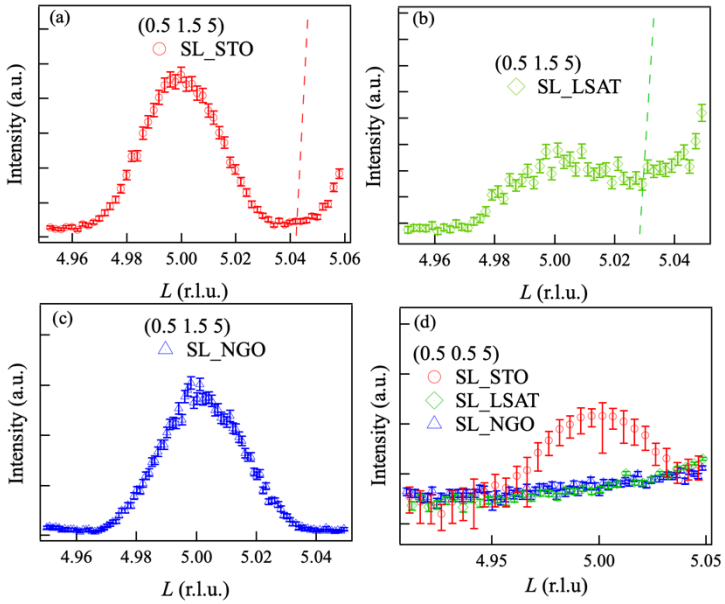

FIG. S3. Room-temperature *L*-scan across the (0.5 1.5 5) Bragg reflection of SL-STO (a), SL-LSAT (b) and SL-NGO (c). (d) *L*-scan across the (0.5 0.5 5) reflection for all the SLs. The Bragg reflection of the SLs were defined using the $a \times a \times 2c$ (a and c are the in-plane and out-of-plane lattice parameters of a pseudo-cubic unit cell, respectively) supercell. The error bar denotes statistical error.

4. X-ray absorption spectroscopy measurements across Ir L-edge.

We measured valence state of Ir through x-ray absorption spectroscopy (XAS) experiments at the Ir L-edge. As shown in Fig. S4, the XAS line shapes of SL-STO and SL-NGO are similar and there is no observable energy shift between them at the L_3-edge. Furthermore, the nominal Ir^{4+} valence state in the SLs can be concluded because of the same XAS line shapes of

the SLs and IrO_2, and an Ir^{3+} valence state will cause a large energy shift of 2 eV as that observed in $IrCl_3$. Due to the strong fluorescence signal from the LSAT substrate around the Ir edge, however, we are not able to measure XAS of the SL-LSAT. Nevertheless, given that all the SLs were prepared under the same condition and the compressive strain of SL-LSAT is in between SL-STO and SL-NGO, we expect the same Ir^{4+} valence state in the SL-LSAT. In addition, we are able to estimate the expectation value for spin-orbit coupling $\langle L \cdot S \rangle$ based on the XAS branching ratio (BR) of the L_3-edge and L_2-edge [8]. The BR, which is the ratio between the integrated while line intensities at the L_3-edge and L_2-edge, is obtained for both SL-STO and SL-NGO [8,9]. Then, we can relate the BR to the $\langle L \cdot S \rangle$ of the holes on Ir 5d orbital states : $BR = (2 + r)/(1 - r)$ where $r = \langle L \cdot S \rangle / \langle n_h \rangle$ [8,10]. Thus, for SL-STO, we obtained $\langle L \cdot S \rangle = 2.65$ ($\hbar^2$) and $\langle L \cdot S \rangle = 2.40$ ($\hbar^2$) for SL-NGO. These values are similar to other iridate compounds with an Ir^{4+} valence state under an octahedral crystal field [4,9,10], confirming the picture of a half-filled pseudospin-half state. The difference between the two samples is within the error of the analysis.

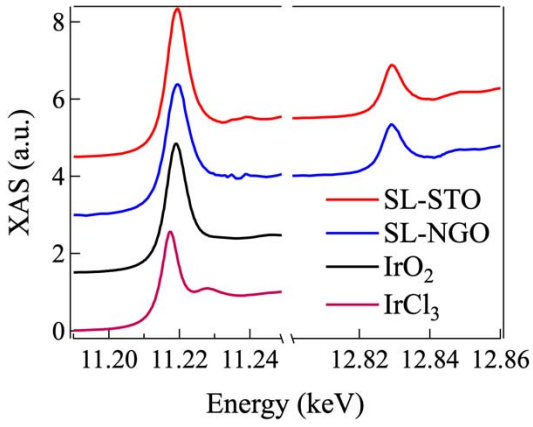

FIG S4. XAS of SL-NGO (blue), SL-STO (red), IrO_2(black) and $IrCl_3$ (pink) at the Ir L_3-edge and L_2-edge. The absorption is shifted vertically for clarity.

5. Details of DFT calculation

The density functional theory (DFT) calculations are performed using the projector augmented wave (PAW) technique as implemented in Vienna ab-initio Simulations Package (VASP) [11]. The Perdew-Burke-Ernzerhof (PBE) functional revised for solids (PBEsol) [12] is used. Plane wave basis set, which are expanded until the cut-off energy of 600 eV, is used to represent the Kohn-Sham wave functions. In the superlattice (SL), since there is a high spin-orbit coupling (SOC) element (Ir), we have included SOC in the calculations. The in-plane pseudocubic lattice parameters of the three SLs at room temperatures are the same as that of the three substrates according to the fully strained state (see the main text). We scale them by a factor of 0.9982 for the calculations since the equilibrium lattice parameter of STO obtained by DFT calculation is 3.898 Å instead of 3.905 Å [13]. The experimental c/a ratios are used for calculations of SLs. The pseudocubic *c*- and *a*-axis lattice parameters of the SLs represent the Ir-Ti and Ir(Ti)-Ir(Ti) interatomic distances, respectively. The atomic positions of the SLs are relaxed in the calculations to find the lowest-energy state. Additionally, to avoid the complications associated with the choice of *U* [6,14-16], we set U to zero in all the calculations. In the calculated structures, the Ir-O-Ti bond angle, which represents the octahedra tilting with respect to the in-plane pseudocubic axes, is 178.4° for SL-STO, 179.8° for SL-LSAT, and 179.8° for SL-NGO. The later two mean the bong angle is effectively 180° within computational error and there is no octahedral tilt, which is consistent with the experimental observation. The Ir-O-Ir bond angle, which is predominantly caused by octahedral rotation with respect to the *c*-axis, is 151.6° for SL-STO, 150.6° for SL-LSAT and 150.1° for SL-NGO. The Ti-O-Ti bond angle is 173.9° for SL-STO, 171.8° for SL-LSAT and 170.4° for SL-NGO.

[1] L. Hao, D. Meyers, C. Frederick, G. Fabbris, J. Yang, N. Traynor, L. Horak, D. Kriegner, Y. Choi, J.-W. Kim, D. Haskel, P. J. Ryan, M. P. M. Dean and J. Liu, Phys. Rev. Lett. **119**, 027204 (2017).
[2] B. J. Kim, H. Ohsumi, T. Komesu, S. Sakai, T. Morita, H. Takagi, and T. Arima, Science **323**, 1329 (2009).
[3] J. W. Kim, Y. Choi, J. Kim, J. F. Mitchell, G. Jackeli, M. Daghofer, J. van den Brink, G. Khaliullin, and B. J. Kim, Phys. Rev. Lett. **109**, 037204 (2012).
[4] S. Boseggia, R. Springell, H. C. Walker, H. M. Ronnow, C. Ruegg, H. Okabe, M. Isobe, R. S. Perry, S. P. Collins and D. F. McMorrow, Phys. Rev. Lett. **110**, 117207 (2013).
[5] H. Sagayama, D. Uematsu, T. Arima, K. Sugimoto, J. J. Ishikawa, E. O'Farrell, and S. Nakatsuji, Phys. Rev. B **87**, 100403 (2013).
[6] J. Matsuno, K. Ihara, S. Yamamura, H. Wadati, K. Ishii, V. V. Shankar, H.-Y. Kee, and H. Takagi, Phys. Rev. Lett. **114**, 247209 (2015).
[7] A. Glazer, Acta Cryst. B **28**, 3384 (1972).
[8] G. van der Laan and B. T. Thole, Phys. Rev. Lett. **60**, 1977 (1988).
[9] J. P. Clancy, N. Chen, C. Y. Kim, W. F. Chen, K. W. Plumb, B. C. Jeon, T. W. Noh, and Y.-J. Kim, Phys. Rev. B **86**, 195131 (2012).
[10] D. Haskel, G. Fabbris, M. Zhernenkov, P. P. Kong, C. Q. Jin, G. Cao, and M. van Veenendaal, Phys. Rev. Lett. **109**, 027204 (2012).
[11] G. Kresse and J. Furthmueller, Phys. Rev. B **54**, 11169 (1996).
[12] J. P. Perdew, A. Ruzsinszky, G. I. Csonka, O. A. Vydrov, G. E. Scuseria, L. A. Constantin, X. Zhou, and K. Burke, Phys Rev Lett **100**, 136406 (2008).
[13] L. Zhang, B. Liu, H. Zhuang, P. R. C. Kent, V. R. Cooper, P. Ganesh, and H. Xu, Comput. Mater. Sci **118**, 309 (2016).
[14] S. J. Moon, H. Jin, K. W. Kim, W. S. Choi, Y. S. Lee, J. Yu, G. Cao, A. Sumi, H. Funakubo, C. Bernhard and T. W. Noh, Phys. Rev. Lett. **101**, 226402 (2008).
[15] B. Kim, P. Liu, and C. Franchini, Phys. Rev. B **95**, 115111 (2017).
[16] S. Y. Kim, C. H. Kim, L. J. Sandilands, C. H. Sohn, J. Matsuno, H. Takagi, K. W. Kim, Y. S. Lee, S. J. Moon and T. W. Noh, Phys. Rev. B **94**, 245113 (2016).